International Journal of GEOMATE, Dec., 2017, Vol. 13, Issue 40, pp. 148-154
Special Issue on Science, Engineering & Environment, ISSN: 2186-2990, Japan
DOI: https://doi.org/10.21660/2017.40.02765

DESIGN AND COMPARISON OF FIVE TOPOLOGIES ROTOR PERMANENT MAGNET SYNCHRONOUS MOTOR FOR HIGH-SPEED SPINDLE APPLICATIONS

*Wawan Purwanto[1], Risfendra[2], Donny Fernandez[3], Dwi Sudarno Putra[4], and Toto Sugiarto[5]

[1,2,3,4,5]Faculty of Engineering, Universitas Negeri Padang, Indonesia

*Corresponding Author, Received: 11 Oct. 2017, Revised: 6 Nov. 2017, Accepted: 26 Nov. 2017

ABSTRACT: The permanent magnet rotor structures had a marked influence on the torque, efficiency, and power density of permanent magnet synchronous motor (PMSM). This paper presents the design and comparison of five different rotor topologies of PMSM. The rotor topologies including surface magnet, decentered magnet, broad-loaf magnet, buried (spoke) magnet, and interior permanent magnet. The optimal design was established using the Taguchi method and finite element analysis (FEA). The purpose of the study was to create a design solution for PMSM rotor with high output power, torque, and efficiency for high-speed spindle applications. The performance characteristics which including magnetic thickness and mass, magnetic flux density, cogging torque, torque and efficiency were compared and analyzed through a two-dimensional (2D) transient FEA, and the feasibility of the rotor designs is validated. The results show that the decentered permanent magnet motor generates the highest magnetic flux density, thus yielding the highest output power, torque, and efficiency.

Keywords: Cogging Torque, Efficiency, Five Rotor Topologies, Taguchi Method, Torque

1. INTRODUCTION

The desired characteristics of a PMSM are high torque, efficiency, and power density [1]-[3]. Furthermore, for the spindle motors, PMSM torque and efficiency must be high in a wide constant power speed range operation. The constant power speed range, torque and efficiency are greatly influenced by the permanent magnet (PM) rotor structures [2]-[6]. Thus, to improve the performance of PM motor by optimizing the rotor design has been widely performed by researchers.

The recent development in PM motor has presented a solution for variable speed operations. Aimeng at al. [2] presented a detailed comparison of the major performance characteristics at variable speed operations of five rotor topologies. In which their advantages and limitations of the rotor were discussed. Michael at al. [7] developed of rotor lamination for high-speed and torque operations. Moreover, through the rotor design, high performance of PM motor can be achieved [3], improve fault tolerance [4], reducing cogging torque [5], and minimization torque ripple [6]. Constant power speed operations can be achieved using optimal field-weakening, through control of the air-gap flux density by modifying the armature reaction demagnetization [7]-[9]. The PMSM rotor structure substantially influenced the constant power speed range, and design optimization of the rotor parameters enhances torque [1]-[8]. PM rotors are classified as surface, segmented, and interior rotors, with each having its unique applications.

Interior PM motor (IPM) have been investigated for hybrid electric vehicle applications [14], [15]. In which the results revealed that SPM and IPM deliver nearly the same output power, however SPM motors are easier to manufacture. IPM motors have enhanced overload capabilities compared with SPM motors. But, IPM motors have higher joule losses at low speeds because of the end connections and the high number of stator slot and rotor segments necessary to regulate harmonic loss, which increases fabrication costs. These characteristics must be considered in the development of high-speed PM rotor. In addition, the location of the rotor magnets has significant effect on the motor mechanical and electrical characteristics, especially on the inductance of the motor [10].

The most crucial point from previous research results are by optimizing the rotor geometry we can optimize the PM motor performance which makes the total loss minimum. Furthermore, the present study design and comparison of five topologies rotor PM motor to improving the performance of a high-speed spindle PMSM for machine tool applications.

This study was started by developing analysis of PMSM. Then, the Taguchi method coupled with FEA were employed to obtain five geometry of PM rotor including surface magnet, decentered magnet, broad loaf magnet, buried (spoke) magnet,

and interior PM rotor.

The objective of this study is to develop PMSM with high output power, torque, and efficiency for high-speed spindle motor applications. Finally, the rotor designs are compared and analyzed their characteristics through a 2D transient FEA. Then, the feasibility of the rotor designs is validated.

2. MATHEMATICAL ANALYSIS AND DESIGN OF PMSM

2.1 Mathematical Analysis

Mathematical analysis of PMSM can be represented as *d*-*q* model [8]:

$$v_{qa} = R_1 i_{qa} + L_q \frac{di_{qa}}{dt} + L_d i_{da} \omega_r + \lambda_f \omega_r \quad (1)$$

$$v_{da} = R_1 i_{da} + L_d \frac{di_{da}}{dt} - L_q i_{qa} \omega_r \quad (2)$$

$$v_a^2 = v_{qa}^2 + v_{da}^2 \quad (3)$$

where v_{qa} and v_{da} are the stator voltage in the q and d-axis, i_{qa} and i_{da} are the stator current in the q and d-axis, L_q and L_d are the inductances in the q and d-axis, λ_f is the armature flux linkage, ω_r is the synchronous electrical speed, R_1 is the stator resistance, and v_a is the rms stator voltage.

For a m_a-phase salient pole, electromagnetic power can be described as [13]:

$$P_e = m_a \left[\frac{V_i E_f}{X_d} \sin\delta + \frac{V_i^2}{2} \left(\frac{1}{X_q} - \frac{1}{X_d} \right) \sin 2\delta \right] \quad (4)$$

where V_i is the input (terminal) voltage, E_f is the electromagnetic force induced by the rotor excitation flux, δ is the power angle, X_d is the synchronous reactance in the d-axis, and X_q is the synchronous reactance in q-axis. Then, by determining electromagnetic power and angular synchronous speed $\omega_s = 2\pi n_s$, the electromagnetic torque can be derived as

$$T_e = \frac{P_e}{2\pi n_s} = \frac{m_a}{2\pi n_s} \left[\left[\frac{V_i E_f}{X_d} \sin\delta + \frac{V_i^2}{2} \left(\frac{1}{X_q} - \frac{1}{X_d} \right) \sin 2\delta \right] \right] \quad (5)$$

Maximizing the electromagnetic torque is crucial to obtain the higher torque and compact size of the PMSM motor. It can be achieved when the torque is handled only in i_{qa} while maintaining i_{da} = 0. Furthermore, maximum torque can be reached by increasing the power electronics as well as air-gap flux, which is determined by rotor and stator geometry, the number of winding turns per slot, slot geometry, and rotor and stator material [13].

2.2 Design of Five Rotor Topologies

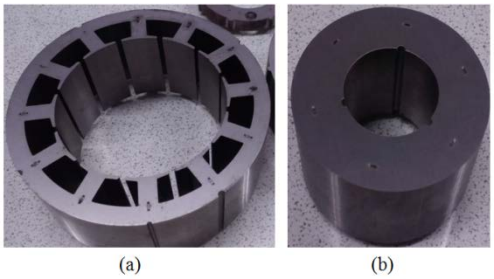

Fig. 1 High-speed spindle PMSM prototype, (a) stator core, (b) decentered magnet PM rotor

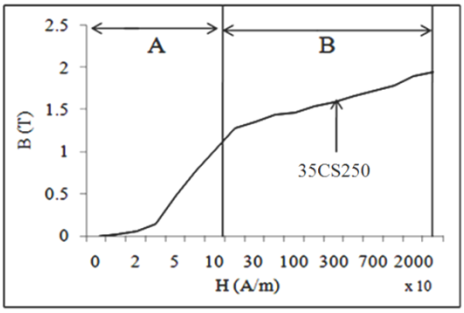

Fig. 2 B-H curve material

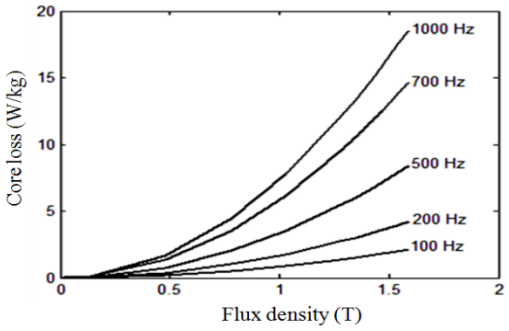

Fig. 3 Core loss of core material 35CS250

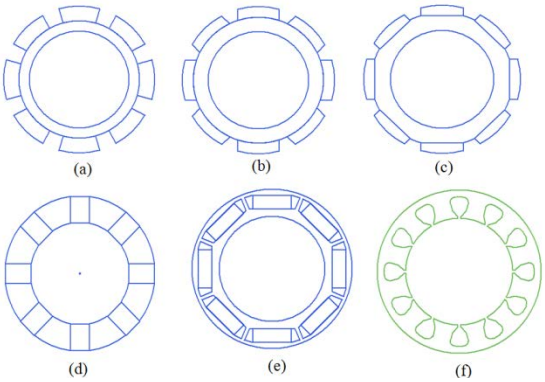

Fig. 4 Five topologies of PM rotor, (a) surface PM, (b) decentered PM, (c) broad loaf PM, (d) buried (spoke) PM, (e) IPM, and (f) stator configuration of PM motor

Fig. 1 shows the prototype of the stator and decentered magnet rotor geometry of high-speed spindle PM motor. The stator and rotor material are silicon electric steel 35CS250 and rotor magnet type is NdFe35. Fig. 2 and 3 provides the B-H curve and stator core loss characteristics of the material. This material exhibits the highest flux density with a low-saturation at Region A. However, it exhibits the lowest saturation flux density in Region B (high-saturation region). Therefore, the material exhibits the highest efficiency when used in Region A because a reduction in current and core loss can be achieved.

Fig. 4 presents the cross-section of the purposed SPM and IPM rotor motor topologies. Fig. 4(a), (b), and (c) show the surface (SPM), decentered (DPM), and broad loaf (DLPM) motors, respectively. Fig. 4(d) and (e) present buried (spoke; (BPM)), and interior (IPM) motors, respectively. The differences between the SPM and IPM rotors are only in the geometry of their magnets in surface rotor area.

Table 1 PMSM Specifications

Parameter	Value
Rated Output Power (kW)	30
Rated Voltage (V)	220
Speed (rpm)	15000
Number of Poles	8
Number of Stator Slots	12
Outer Diameter of Stator (mm)	120
Inner Diameter of Stator (mm)	79
Length of Stator Core (mm)	120
Outer diameter of rotor (mm)	69.5
Inner diameter of rotor (mm)	46.5
Length of rotor (mm)	120

Table 1 lists the specifications of the PM motor used in this study. The Taguchi method is used to obtain the optimal combination of the five rotor topologies. The Taguchi method uses five factors and five levels for all rotor designs, and the standard Taguchi method orthogonal array L25 (5^5) is used [11], [12], with efficiency and torque as the objective functions. Spindle motor performance in L25 matrix experiments are obtained using 2D FEA. The optimal combination of the rotor geometries are determined using response table, effect plots, and analysis of variance (ANOVA) drawn from the matrix experiments as developed in [16], [17]. The obtained optimal combination is verified using FEA as described [18]. The optimization results are listed in Table 2. To make a fair comparison for five rotor designs, and to ensure, that the performance characteristics as output power, torque, efficiency, and magnetic flux density are only defined and controlled by PM rotor geometry, we use the stator winding configuration is fixed, same rated voltage, frequency, output power, stator and rotor core material, and rotor magnet type.

Table 2 Optimization Results

Parameters	PM Rotor				
	SPM	DPM	DLPM	BPM	IPM
Rotating angle on basis of center of PM motor (^{0})	10	12	8	10	10
Magnet thickness (mm)	7	5	5	6	4
Wide of magnet (mm)	17	18.5	18	9	16
Rotor Length (mm)	130	120	120	110	120
Air gap length (mm)	0.5	0.6	0.8	0.8	0.5

3. PERFORMANCE ANALYSIS AND COMPARISON

3.1 Magnetic Thickness and Mass

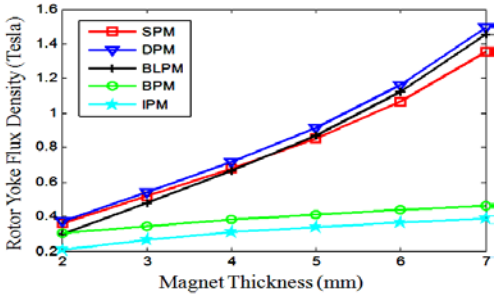

Fig. 5 Rotor yoke flux density with magnetic thickness

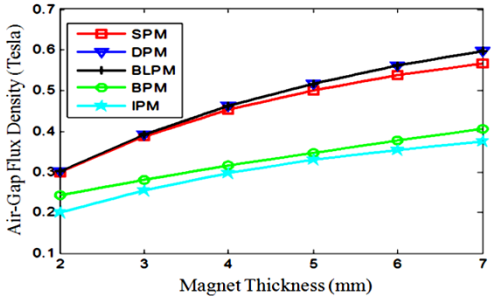

Fig. 6 Air gap flux density with magnet thickness

Magnet thickness of the PM rotor is closely associated with the rotor yoke flux density, air-gap

flux density, and armature copper loss. Magnet mass is closely related with *q* and *d*-axis line currents and maximum line induced voltage. It affects the torque generated by the PM motor [2], [15]. Fig. 5 compares magnet thickness and rotor yoke flux density. In the SPM, DPM, and BLPM, magnet thickness considerably influences rotor yoke flux density, which is not the case in the BPM and IPM.

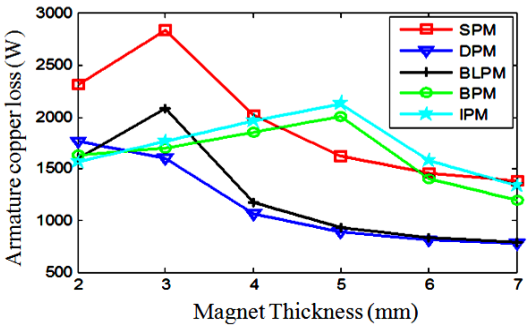

Fig. 7 Armature copper loss with magnet thickness

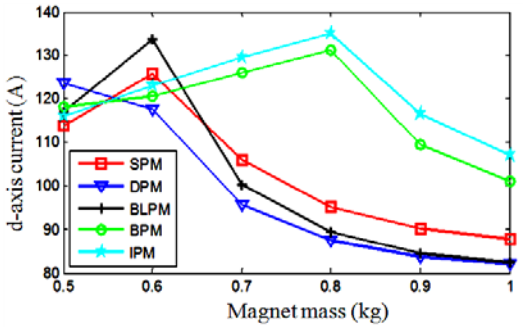

(a)

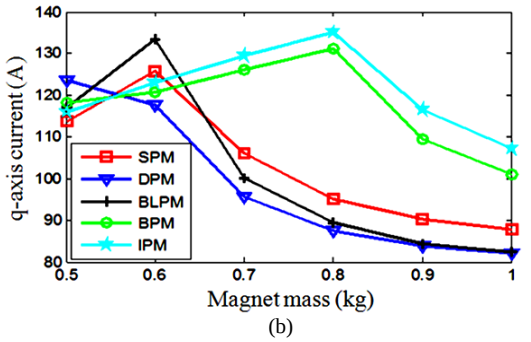

(b)

Fig. 8 *d* and *q*-axis current with magnet mass, (a) *d*-axis current, (b) *q*-axis current

In addition, magnet thickness influences air-gap flux density of the SPM, DPM, and BLPM as shown in Fig. 6. An increase in magnetic thickness will reduce the armature copper losses in the SPM and DPM, respectively, as shown in Fig. 7. Moreover, magnetic mass increases with increasing magnetic thickness. In the SPM, DPM, and BLPM, *d* and *q*-axis currents decrease with increasing magnetic mass, as shown in Fig. 8 (a) and (b). In the PMSM, magnetic mass affects the maximum induced voltage. The magnetic mass of the five rotor topologies increases the induced voltage, shown in Fig. 9.

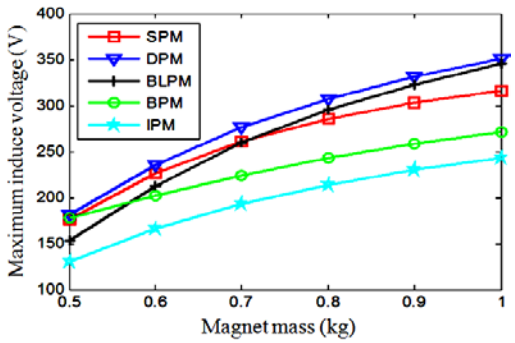

Fig. 9 Maximum induce voltage with magnet mass

Table 3 Magnet Mass and Dimension

Topology	Magnet thickness (mm)	Mass (kg)	Width of magnet (mm)
SPM	7	0.81	17
DPM	5	0.97	18.5
BLPM	5	1.08	18
BPM	6	1.11	9
IPM	4	0.997	16

Table 4 Performance Comparison

Parameter	SPM	DPM	BLPM	BPM	IPM
Output Power (kW)	30	30	30	29.8	30
Efficiency (%)	90.58	93.1	92.1	91.94	90.26
Torque (Nm)	19.1	23.88	19.1	18.97	19.1
Frictional and Windage Loss (W)	160	160	160	160	160
Iron-Core Loss (W)	162.08	162.67	149.22	121.42	83.25
Armature Loss (W)	1461.22	895.72	933.02	1194.2	1583.61
Total Loss (W)	1783.3	1218.39	1242.24	1475.62	1826.86

Table 3 summarizes the magnet thickness and mass of the five optimized rotor topologies. The magnetic thickness and mass necessary for obtaining optimal performance in each rotor topology as reported in Table 4.

3.2 Magnetic Flux Density

Magnetic flux density is a crucial parameter in PM motor design. Increasing the magnetic flux density increases output power and efficiency, and the magnet thickness affects the magnetic flux

density, as shown in Fig. 10. The influence of magnet thickness on magnetic flux density is the highest in the IPM. Fig. 11 and 12 show that increase in magnetic flux density improves the torque and efficiency. In all five rotor topologies, the magnet thickness affects magnetic flux density, torque, and efficiency.

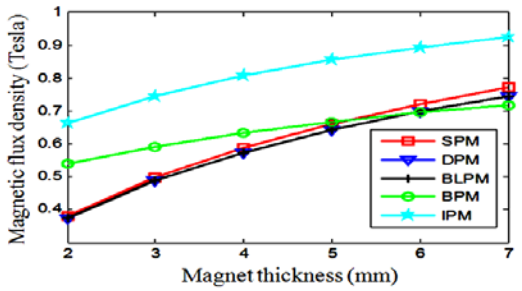

Fig. 10 Magnet flux density with magnet thickness

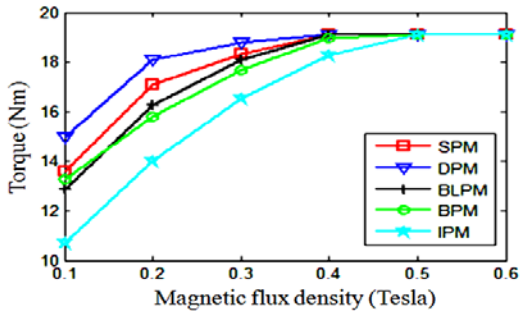

Fig. 11 Torque with magnet Flux density

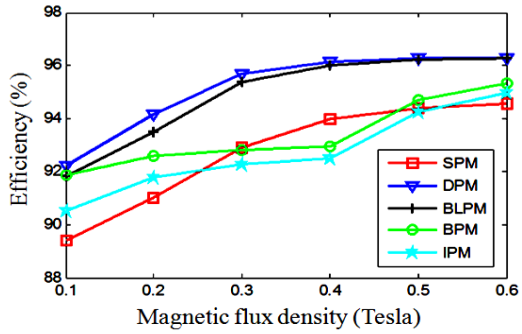

Fig. 12 Efficiency with magnet flux density

The variation of the magnetic flux density with electric angle is shown in Fig. 13. The BPM and IPM difference in the direction of their electric angles, with the SPM, DPM, and BLPM, it is consistent with the characteristics of IPM motors. The FEA result of magnetic flux density is depicted in Fig. 14. Generally, strong magnetic flux density is generated in the magnet surface. The DPM motor (Fig. 14(b)) generates a strongest flux density. The IPM magnetic flux density is the lowest. The higher concentration of flux density the SPM, DPM, and BLPM afford to output power and electric angle compared with the BPM and IPM, as shown in Fig. 15.

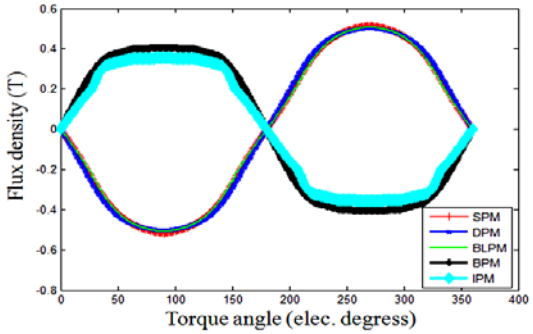

Fig. 13 Magnet flux density with torque angle

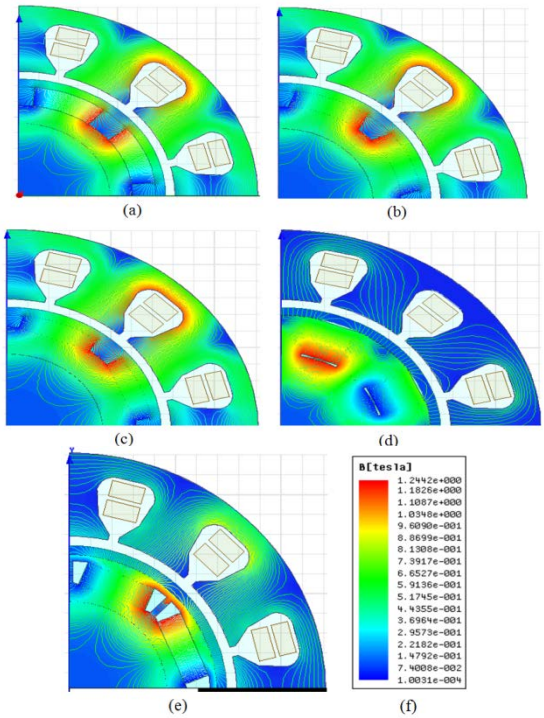

Fig. 14 Magnetic flux distribution for no-load condition, (a) SPM motor, (b) DPM motor, (c) BLPM motor, (d) BPM motor, (e) IPM motor, (f) scale.

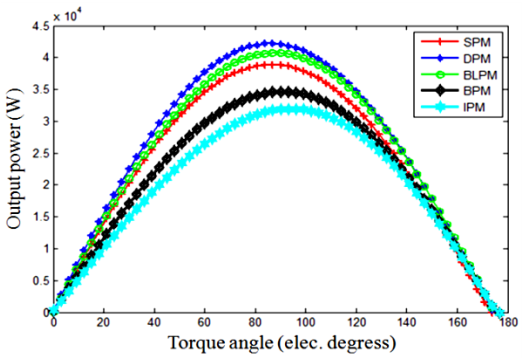

Fig. 15 Output power with torque angle

3.3 Performance Characteristics

The five rotor designs are analyzed for constant-power speed operation through 2D

transient FEA [18], and the performance characteristics reported in Table 4. The DPM rotor produces the highest torque, and the BPM rotor produces the lowest torque, as shown in Fig. 16 and Table 4.

Cogging torque is caused by the interaction between the permanent magnet in the rotor and the stator slots of the PM motors. The cogging torque is essential in optimal PMSM rotor design. Cogging torque causes torque ripples, vibrations, and mechanical noise [15]. The cogging torques of five rotor topologies presented in Fig. 17. The IPM produces the lowest cogging torque (0.12 Nm), whereas the highest cogging torque (0.21 Nm) is generated by the BPM rotor as shown in Fig. 18.

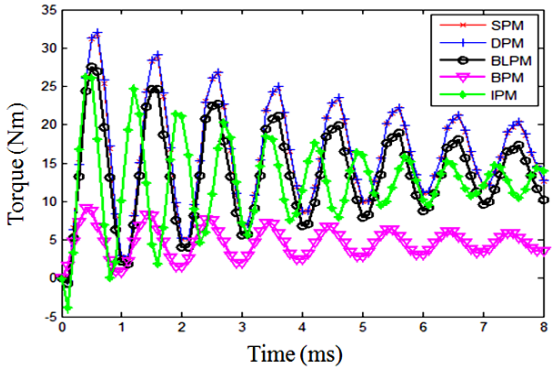

Fig. 16 Comparison of torque profile

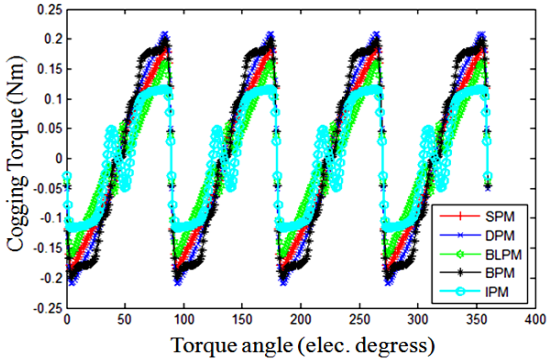

Fig. 17 Cogging torque profile

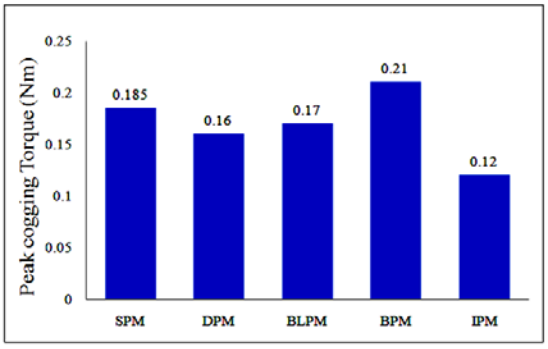

Fig. 18 Peak cogging torque

Increased in output power indicates to higher motor efficiency, that is optimal input energy conversion. The SPM rotor exhibits the lowest efficiency because of high total loss which leads to high armature thermal load, current density, and specific electric loading. The Stator current waveform affects the total loss in PMSM. The higher current waveform in IPM triggers higher in armature thermal load, which is highest in the IPM rotor of 1511 A^2/mm^3 and lowest in the DPM of 854 A^2/mm^3. The highest current waveform also causes specific electrical loading. The armature current density is highest in the BPM of 58.65 A/mm and lowest in the IPM of 22.38 A/mm^2. The lowest specific electrical loading and armature current density occurs in the DPM of 50.8 A/mm and 16.83 A/mm^2 as listed in Table 5.

Table 5 Current Performance

Parameter	SPM	DPM	BLPM	BPM	IPM
Armature Thermal Load (A^2/mm^3)	1134	854	890	1140	1511
Specific Electric Loading (A/mm)	52.35	50.8	51.84	58.65	67.54
Armature Current Density (A/mm^2)	21.67	16.83	17.18	19.43	22.38

4. CONCUSION

This paper presents the design and performance comparison of five PM rotor topologies including magnet thickness, mass, and magnetic flux density. The Taguchi method and 2D FEA are used in the designs optimization and performance analysis. The results are DPM with a magnetic thickness of 5 mm produces the higher magnetic flux density and the lowest armature copper loss. Whereas the IPM with a magnet thickness of 6 mm produces the lowest magnetic flux density and higher armature copper loss. The DPM generates the highest magnetic flux density, thus yielding the highest output power, torque, and efficiency. However, BPM is produces higher cogging torque with the IPM producing is the lowest. In the IPM, the higher waveform current improves the armature thermal load, current density and specific electric loading. Based on the comparison and analysis results, the DPM motors are recommended for spindle PM motors requiring high torque and efficiency and low cogging torque. In future work, the present study results will be verified and compared through a prototype high-speed PM motor with decentered rotor.

5. REFERENCES

[1] H. K. Yeo, D. K. Woo, D. K. Lim, J. S. Ro, and H. K. Jung, "Analysis of a surface-mounted permanent-magnet machine with overhang structure by using a novel equivalent magnetic circuit model", Journal of Electrical Engineering and Technology, vol. 9, no. 6, pp. 1960-1966, 2014.

[2] A. Wang,Y. Jia, and W. L. Soong, "Comparison of five topologies for an interior permanent-magnet machine for a hybrid electric vehicle", IEEE transactions on Magnetics, vol. 47, no. 10, pp. 3606-3609, 2011.

[3] K. C. Kim, Ju Lee, Hee Jun Kim, and Dae-Hyun Koo, "Multiobjective Optimal Design for Interior Permanent Magnet Synchronous Motor", IEEE Transactions on Magnetics, vol. 45, no. 3, March 2009, pp. 1780-1783.

[4] Q. Chen, G. Liu, L. G. Sun, Y. Jiang, and J. Yang, "Comparison of Five Topologies Rotor Permanent Magnet Motors with Improved Fault-Tolerance", Industrial Electronics (ISIE), 2013 IEEE International Symposium, Taiwan, 2013, pp. 1-5.

[5] M. H. Yoon, D. Y. Kim, S. I. Kim, and J. P. Hong, "An Asymmetric rotor design of interior permanent magnet synchronous motor for improving torque performance", Journal of magnetic, vol. 20, no. 4, pp. 387-393, 2015.

[6] P. Zhang, G. Y. Sizov, N. A.O. Demerdash, "Comparison of torque ripple minimization control techniques in Surface-Mounted Permanent Magnet Synchronous Machines", 2011 IEEE International Electric Machines & Drives Conference (IEMDC), Niagara falls, pp. 188-193, 2011.

[7] H. Hwang, J. Hur, and C. Lee, "Design and analysis of a permanent-magnet-assisted switched reluctance motor", Journal Electrical Engineering and Technology, vol. 9, no. 6, pp. 2209-2217, 2014.

[8] M. Soshi, S. Yu, S. Ishii, and K. Yamazaki, "Development of a high torque–high power spindle system equipped with a synchronous motor for high performance cutting", CIRP Annals - Manufacturing Technology vol. 60, pp. 399–402, 2011.

[9] C. M. Kim, D. Y. Kim, G. W. Cho, and G. T. Kim, "The design of flux barrier for improvement of demagnetization endurance in BLDC motor", Journal of Electrical Engineering and Technology, vol. 9, no. 6, pp. 2181-2186, 2014.

[10] H. K. Patel, R. Nagarsheth, and S. Parnerkar, "Performance comparison of permanent magnet synchronous motor and induction motor for cooling tower application, "International Journal of Emerging Technology and Advanced Engineering", vol. 2, no. 8, pp. 167-171, 2012.

[11] W. Y Folkers and C. M. Creveling, Engineering Method for robust product design, Addison–wesley publisher company, 3rd print, 1998.

[12] M. S, Phadke, Quality engineering using robust design, Prentice hall, 1989.

[13] J. F. Gieras, Permanent magnet motor technology design and application", CRC Press, New York, 2010.

[14] G. Pellegrino, A. Vagati, P. Guglielmi, and B. Boazzo, "Performance Comparison Between Surface-Mounted and Interior PM Motor Drives for Electric Vehicle Application", IEEE Transactions on Industrial Electronics, vol. 59, no. 2, pp. 803-811, 2012.

[15] A. Vagati, G. Pellegrino, and P. Guglielmi, "Comparison between SPM and IPM motor drives for EV application", XIX International Conference on Electrical Machines - ICEM 2010, Rome, pp. 1-6, 2010.

[16] N. Bala, M. Napiah and I. Kamaruddin, "Application of Response Surface Methodology for Mix Design Optimization of Nanocomposite Modified Asphalt Mixtures", International Journal of Geomate, vol.13, no. 39, pp.237-244, 2017.

[17] R. Lee and I. Y. Chen, "A Novel Production Process Modeling for Analytics" International Journal of Geomate, vol. 11, no. 24, pp. 2370-2377, 2016.

[18] Ansoft Maxwell user's guidance ver. 14, ANSYS Inc, Southpointe, Canonsburg, USA. 2010